

Numerical Simulation of Detonation Processes in a Variable Cross-Section Chamber

H. Y. Fan* and F.K. Lu†

*Aerodynamics Research Center, Mechanical and Aerospace Engineering Department,
University of Texas at Arlington, Arlington, TX 76019-0018, USA*

The detonation processes occurring in a combustion chamber with variable cross-sections are numerically simulated for a hydrogen-air reacting flow. The chamber consists of a large diameter tube and two small identical tubes connected on each side through frustums. The channel is closed at the left end and opened at the right. A two-dimensional, time accurate, finite-volume-based method is used to perform the computations. A five-species, two-step global reaction mechanism is used. Two detonation cases are simulated, corresponding to initiation from the closed, left end and the opened, right end. The study showed that area change gave rise to complex wave phenomena. The area change and wave reflections yielded extreme parameters.

I. Introduction

GASEOUS detonations, with their terrifyingly destructive nature, can nonetheless be exploited for many positive purposes. This subject has received considerable interest for certain applications, such as in propulsion¹ and in high-enthalpy ground test facilities.² The primary advantage of detonation combustion as compared to deflagration is its rapid energy release. This rapid energy release allows the design of pulse detonation engines with high specific power. While there are many unresolved fundamental issues regarding initiation, transition and propagation, for example, numerical modeling for obtaining engineering solutions can be sought for the above-mentioned applications. Time-accurate computational fluid dynamics (CFD) methods can be used to perform cycle analysis and design optimization. An unsteady numerical simulation model was proposed for the purposes described above.³ This two-dimensional, time-accurate, finite-volume-based model has been demonstrated with different example cases to formulate the physical detonation phenomena precisely, including chemical and thermal non-equilibrium.

Most pulse detonation studies, both experimental and numerical, up to date have been performed on simple configurations, namely, a tube of constant cross section.¹ In contrast, Baklanov et al.⁴⁻⁶ recently performed an experimental study of detonation with variable cross-section chambers. Balkanov et al. found the possibility of producing flow parameters more extreme than those behind a stationary detonation wave.

Besides the above experimental study, no other studies, including numerical ones, have been reported on such a configuration, at least to the authors' knowledge. In our current study, the detonation processes occurring in a variable cross-section chamber are simulated for a hydrogen-air reactive flow with the numerical method developed in.³ The axisymmetric chamber is formed from a main chamber with a large internal diameter, and two small identically sized tubes that are connected on each side of the main chamber through transitional frustums. The entire configuration is closed at one end and opened at the other end. The reaction mechanism is a five-species, two-step global model. The simulation of detonation processes with different initiating locations is carried out. The work is an attempt to obtain a qualitative understanding of detonation phenomena in the variable cross-section chamber through the numerical simulation.

*Visiting Researcher

†Professor, Associate Fellow AIAA

II. Formulation of the Problem

In the present simulation, the time-dependent two-dimensional Euler equations are used to describe an inviscid, non-heat-conducting, reacting gas flow in which thermal non-equilibrium is modeled with a two-temperature model. For simplicity, these equations are described in the Cartesian coordinate system as

$$\frac{\partial U}{\partial t} + \frac{\partial F}{\partial x} + \frac{\partial G}{\partial y} = S \quad (1)$$

where U is the vector of conserved variables, F and G are the convective flux vectors, and S is the vector of source terms:

$$U = \begin{bmatrix} \rho_s \\ \rho u \\ \rho v \\ \rho e_v \\ \rho E \end{bmatrix}, \quad F = \begin{bmatrix} \rho_s u \\ \rho u^2 + p \\ \rho uv \\ \rho u e_v \\ \rho u E + pu \end{bmatrix}, \quad G = \begin{bmatrix} \rho_s v \\ \rho uv \\ \rho v^2 + p \\ \rho v e_v \\ \rho v E + pv \end{bmatrix}, \quad S = \begin{bmatrix} w_s \\ 0 \\ 0 \\ w_v \\ 0 \end{bmatrix} \quad (2)$$

The subscript $s=1, 2, 3, \dots, N_s$ where N_s is the number of species. The first N_s rows represent species continuity, followed by the two momentum conservation equations for the mixture. The next row describes the rate of change in the vibrational energy, and the final row is the total energy conservation equation. The terms u and v are the velocities in the x and y directions respectively, $\rho = \sum_{s=1}^{N_s} \rho_s$ is the mixture density, ρ_s is the density of species s , p is the pressure, e_v is the vibrational energy, E is the total energy per unit mass of mixture, w_s is the mass of production rate of species s per unit volume, and w_v is the vibrational energy source.

The internal energy based on the two-temperature model is assumed to comprise of an \square equilibrium portion at the translational temperature T and a nonequilibrium portion at the vibrational temperature T_v , and can be defined as

$$e = e_{eq}(T) + e_v(T_v) \quad (3)$$

where e_{eq} and e_v are the \square equilibrium and nonequilibrium portions of the internal energy. These energy components can be determined with certain thermodynamic relations.³ The source terms for the species mass production rate in the chemical reactions can be written as⁷

$$w_s = M_s \sum_{r=1}^{N_r} (\beta_{s,r} - \alpha_{s,r})(R_{f,r} - R_{b,r}) \quad (4)$$

where M_s is the molecular weight of species s , N_r is the number of reactions, $\alpha_{s,r}$ and $\beta_{s,r}$ are the stoichiometric coefficients for reactants and products, respectively, in the r th reaction. The forward and backward reaction rates of the r th reaction are $R_{f,r}$ and $R_{b,r}$ respectively. These rates can be determined by the Arrhenius law.³ The source term of vibrational energy can be written as

$$w_v = \sum_s Q_{v,s} + \sum_s w_s e_{v,s} \quad (5)$$

The first term on the right hand side $Q_{v,s}$ represents the vibrational energy exchange rate of species s due to the relaxation process with translational energy which can be determined by the Landau–Teller formulation.^{3,8,9,10} The

second term $w_s e_{v,s}$ represents the amount of vibrational energy gained or lost due to production or depletion of species s from chemical reactions.³

As mentioned above, the algorithm that is used to solve these equations numerically was described in Ref. 3. This algorithm is finite-volume based. The advantage of this method is its use of the integral form of the equations, which ensures conservation, and allows the correct treatment of discontinuities. Nonequilibrium flows involving finite-rate chemistry and thermal energy relaxation often can be difficult to solve numerically because of stiffness. The method includes a point implicit treatment of source terms to reduce the inherent stiffness of the system by effectively rescaling all the characteristic times in the fields into the same order of magnitude. Roe’s flux-difference split scheme^{11,12} is combined with the Runge–Kutta integration schemes for second-order accuracy in capturing the shock waves in space and time.

In the current study, the hydrogen-air combustion mechanism of five-species (N_2 , O_2 , H_2 , H_2O and OH) and two-reactions ($H_2 + O = 2OH$ and $2OH + H_2 = 2H_2O$) proposed by Rogers and Chinitz¹³ is used. This model was developed to represent hydrogen-air chemical kinetics with as few reaction steps as possible while still giving reasonably accurate global results. In this model, nitrogen is counted as a collisional partner in the thermodynamic model and relaxation process, but not included in the chemical reaction model since the maximum temperature in the hydrogen-air reaction does not reach the dissociation temperature of nitrogen.

A novel aspect of the numerical method is a “local ignition averaging model” (LIAM) applied to the global two-step reaction mechanism. As was shown in Ref. 3, for the hydrogen-air reaction process, the mass fraction of some species could change very quickly as soon as the ignition is started. For example, the OH production reaction was instantaneous at its initial stage and went to equilibrium very fast in less than 10^{-12} s. This fact indicates that to ensure that the chemical kinetics are properly followed, the time step in the flow solver should be 10^{-12} s or less. But, it is practically impossible to use this small time step in the flow solver since 10^9 integration steps might be needed to solve a typical detonation wave propagation problem with time scales of 10^{-3} s. The number of steps would result in 10^4 days of CPU time when 1 s of CPU time per computation cycle (which is a proper estimate for this code on a typical front-end workstation) is assumed. This causes a stiffness of the chemical reaction model, which cannot be taken care of by the aforementioned point implicit treatment of source terms. To deal with this stiffness problem, a special treatment is required for the ignition cells. For this purpose LIAM was proposed. The basic idea for this approach comes from the fact that the species mass fractions are changing drastically in a very short period as soon as ignition starts and reaches equilibrium soon afterwards. LIAM separates the cell in which the ignition condition is met and then integrates the chemical kinetics equations alone in that cell. A much smaller time step (e.g. $<10^{-12}$ s) is used in the integration within the interval of the flow solver time step. The average production rate of each species during this time interval is then obtained through dividing the density change of species by the flow solver time step³.

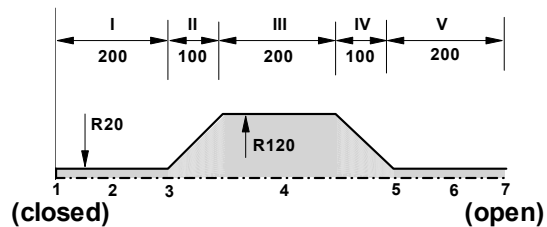


Figure 1: Schematic of the variable cross-section detonation chamber: the main chamber has a 120 mm internal radius and a 200 mm length; small tubes in both sides of the main chamber have 20 mm internal radius and 200 mm length; 1, 2, ..., 7, indicate horizontal locations used for displaying data of interest.

III. Configuration and Computational Setup

The chosen numerical method is applied to simulate detonation wave propagation occurring in an axisymmetric chamber. Figure 1 is a schematic of the configuration. The main chamber (segment III) has a 120 mm internal radius and a 200 mm length, while the small tubes (segments I and V) arranged on both sides of segment III have a 20 mm internal radius and a 200 mm length. The total length of the chamber is 800 mm. The chamber’s left end is closed and the right end is opened. The chamber is initially filled with a homogeneous stoichiometric hydrogen-air mixture at ambient condition (0.101325 MPa and 298.15 K). The detonation wave is initiated inside the chamber at two different positions—in the closed end of the detonation chamber, denoted as the Left Ignition case, and in the

open end of the detonation chamber, denoted as the Right Ignition case. The detonation products expand from the chamber to the surrounding air directly.

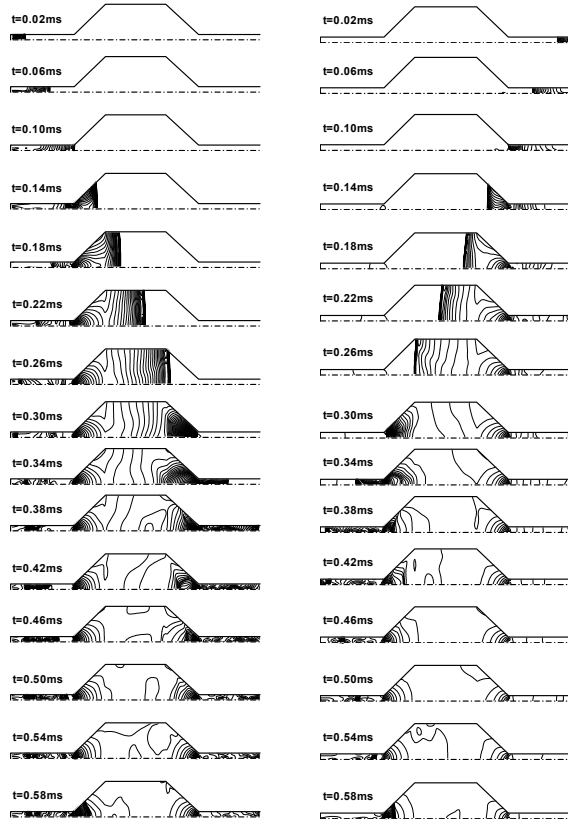
In our current study, a “one-shot” detonation process is simulated. The different parts of the computational domain are meshed with structured grids, which are not all identical. In total, 30×400 cells are set up for the simulation. The “equilibrium hot spot” (EHS) ignition approach³ is applied to initiate detonation wave. For example, in the Left Ignition case, 5 columns of cells adjacent to the closed end wall and 10 rows of cells adjacent to the chamber centerline, in total 5×10 cells, are taken as ignition cells. Similarly, for the Right Ignition case, a cluster of 5×10 cells adjacent to the exit plane and the centerline of the detonation chamber are taken as ignition cells. For both simulation cases, the flow solver time step is 10^{-7} s.

IV. Results and Discussion

A. Overall Observation of Detonation Wave Propagation

The propagation of the simulated detonation wave is first presented as the temporal evolution of the computed pressure fields. The associated contours at different times are shown in Fig. 2. The figure clearly shows the propagation of various disturbances, including the detonation waves. Further, the evolution of spatial distributions of pressure and temperature along the centerline and the chamber wall as the detonation wave develops in the chamber is shown in Fig. 3. From these figures, a general tendency on the intensity of the detonation wave for the two simulated cases can be observed. In each case, the detonation wave, initiated from the ignition spot, very rapidly reaches the Chapman-Jouguet (CJ) state (in our current case, the CJ state is: $p_{CJ} = 1.586$ MPa; $T_{CJ} = 2958$ K;

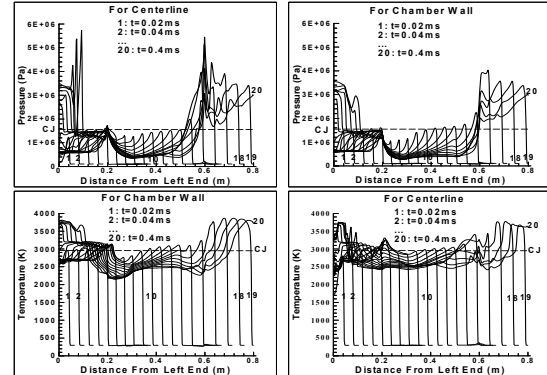
$\rho_{CJ} = 1.54$ kg/m³ and $D_{CJ} = 1977$ m/s) and becomes



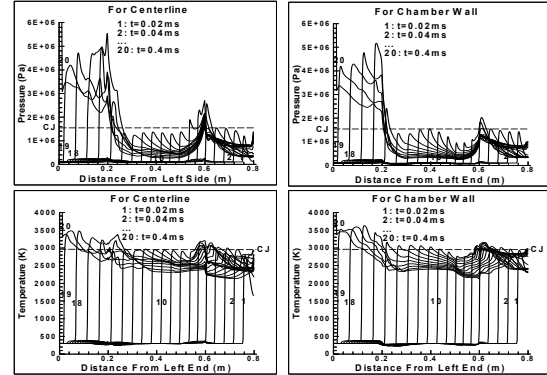
(a) Left Ignition

(b) Right Ignition

Figure 2: Pressure contours with data at $t = 0.02-0.58$ ms at 0.04 ms interval.



(a) Left Ignition



(b) Right Ignition

Figure 3: Evolution of spatial distributions of pressure and temperature along the centerline and the wall of the detonation chamber, with data at $t = 0.02-0.60$ ms at 0.02 ms.

established in the small tube in which it is initiated. The wave then exits the small tube and enters the main chamber. The wave intensity decays to below the CJ state. This intensity decrease seems to occur first near the chamber wall. Nevertheless, as the detonation wave moves forward within the main chamber the intensity of the wave recovers. In other words, there appears to be a re-transition. For the Left Ignition case, the re-transition returns the wave to the CJ state. For the Right Ignition case, the wave only recovers slightly and does not completely reach the CJ state. A further abrupt increase in the intensity of the detonation wave appears when its front passes through the converging part (segment IV for Left Ignition and segment II for Right Ignition, respectively). In accordance with the re-transition phenomenon of the detonation wave in the main chamber, our simulation results indicate that the detonation wave is separated into a shock wave and a flame front. We use pressure to record the shock wave front and oxygen fraction to record the flame front. The temporal evolution of the detonation wave front is re-drawn in Fig. 4. From the figure, we find that a separation of the detonation wave front

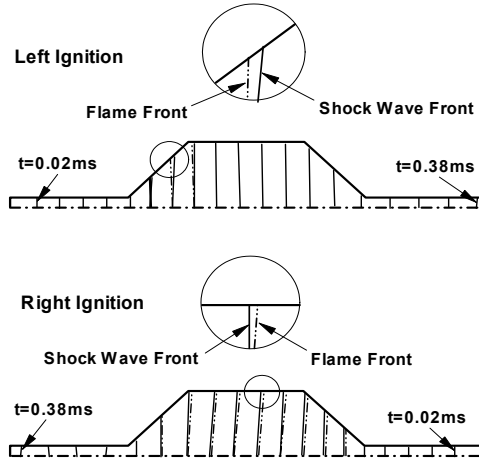


Figure 4: Evolution of detonation wave front at $t = 0.02$ - 0.38 ms at 0.02 ms interval. Pressure is used to record the shock wave front (solid line) and oxygen fraction the flame front (dash-dot line).

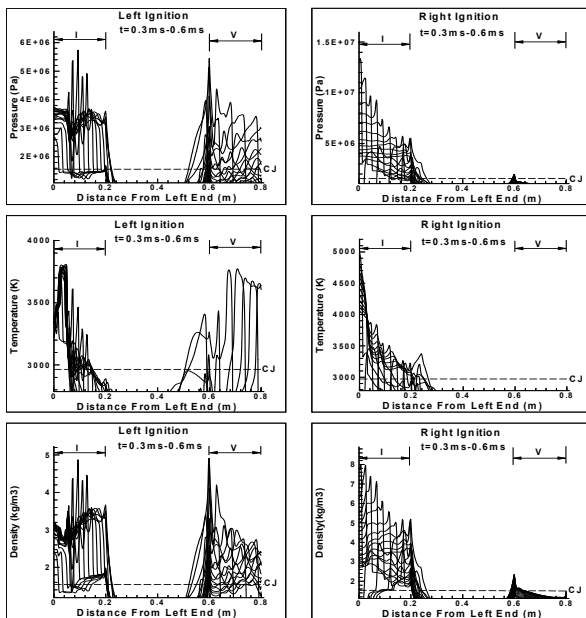


Figure 5: Peaks of extreme parameters (pressure, temperature and density) appearing in the small tubes along the chamber centerline in the two detonation processes for $t = 0.30$ - 0.60 ms at 0.02 ms interval.

appears in both cases: for the Left Ignition case, the separation occurs only in a very small region just within or near the divergent part, while for the Right Ignition case, the separation can be found in a large region through the main chamber. The intensity of the propagating detonation wave continues to increase drastically above the CJ state. The detonation wave then enters into the small tube downstream (segment V for Left Ignition and segment I for Right Ignition, respectively) and propagates through it, sustaining a higher intensity.

It can be noted that the above detonation propagation situation qualitatively supports the observations of Baklanov et al.,⁴ where one of their experimental cases is similar to our current Left Ignition case in geometric configuration and detonation procedure. Baklanov et al.'s measurement results showed that when a well-developed detonation wave in a small tube area enters a large chamber through a divergent section, the wave degenerates and splits into a shock wave and a separate flame front. As the shock wave moves forward and further passes through the

subsequent convergent part, the detonation wave can be re-initiated by a Mach reflection of the shock wave at the convergent part. Hence, this detonation wave enters the subsequent small tube with a high intensity. In comparing with the results of Ref. 4, our computed detonation wave showed a weaker separation phenomenon. In addition, our simulated cases also do not reproduce the fact that the detonation wave is re-initiated by a Mach reflection of the shock wave on the convergent part. However, the intensity variation of the computed detonation wave in our cases still shows a tendency strongly similar to the experimental observations of Ref. 4.

B. Extreme Parameters and Detonation-Induced Waves

The simulation results from the two ignition cases show that, as already mentioned above, extreme parameters can be obtained due to area reduction. These parameters can be many times higher than those of the CJ state. This fact can be seen in Figs. 2 and 3, and are more clearly presented in Fig. 5. In the latter figure, three parameters, viz., pressure, temperature

and density are used to illustrate the super-CJ state, with peaks appearing in the small tubes at $t = 0.3\text{--}0.6$ ms. During this time, the detonation wave exits the main chamber and is passing through the corresponding small tubes. Moreover, during this period, for the Left Ignition case, as the detonation wave strengthens in segment V, a wave reflection occurs in segment I. It can be noted that for the Left Ignition case, high parameters appear in both of the small tubes (segments I and V) whereas, for the Right Ignition case, the high values only mainly appear in the small tube area (segment I).

The increase of the intensity of the detonation wave as it enters an area contraction can be attributed to the geometry. In particular, extreme parameters appearing in the small tube area in segment V for the Left Ignition case is chiefly caused by the convergent part (segment IV), while those in the small tube point area in segment I for the Right Ignition case is partially caused by the convergent part (segment II). (It will be shown later that there are also other reasons yielding the increase of parameters in this area in the latter case.) Baklanov et al.⁴ stated that a convergent part could induce Mach reflection to compress the gas, thereby re-igniting the gas to produce a second detonation. However, in each of our simulated cases, the detonation wave is already recovered before it approaches into the convergent part. Hence, the simulations did not reveal a Mach reflection phenomenon and, thus, we do not observe re-ignition due to Mach reflection. Nevertheless, the simulations show an abrupt increase of the intensity of the detonation wave as it enters the convergent part of the chamber. In other words, the area reduction compresses the gas. This implies that the area reduction is an important contributor to the extreme parameters in the subsequent wave propagation in the small tube. It should be mentioned here that our simulation revealed a strong compression of the combustion products behind the detonation wave within the area reduction that is similar to the compression effect of a Mach reflection. However, the simulation is unable to resolve any Mach reflection and a finer grid may be required.

Moreover, our simulation results show that there are various complicated reasons behind the extreme parameters in the small tube areas. Generally, the waves induced during the detonation propagation contribute to the extreme parameters in the small tubes. In our current study, we only focus on the easily observed waves that are deemed to have a larger effect on the extreme parameter phenomenon.

In our simulation, seven locations, as shown in Fig. 1, are selected along the centerline of the detonation chamber for further analysis. Interesting flow features, such as shock and detonation fronts, are tracked and displayed in Fig. 6. Wave propagation is displayed in Fig. 7. In these two figures, the detonation wave is represented by the line A1-A2-...-A7 for the Left Ignition case and the line A1'-A2'-...-A7' for the Right Ignition case. The detonation wave propagates in the detonation chamber with a velocity approximately equal to the CJ ($D_{CJ}=1977$ m/s) in both ignition cases. These waves are of course the driver of the whole detonation process and the first cause of the extreme parameters in the detonation chambers, especially in the small tubes.

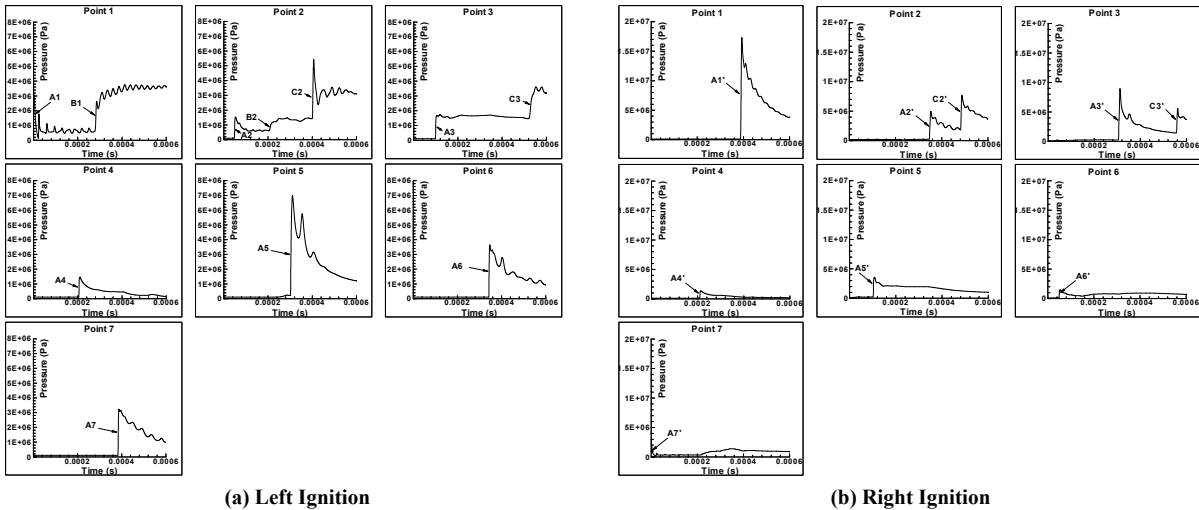


Figure 6: Temporal evolution of pressure at seven locations (see Fig. 1) along the centerline of the detonation chamber: A1, A2, ...A7, and A1', A2', ..., A7' indicate the pressure increases caused by the detonation wave in the Left Ignition and Right Ignition cases, respectively; B1 and B2 indicate the pressure increases caused by a reflected wave, and C2, C3 by a secondary reflected wave, in the Left Ignition case; C2' and C3' indicate the pressure increases caused by a reflected wave in the Right Ignition case.

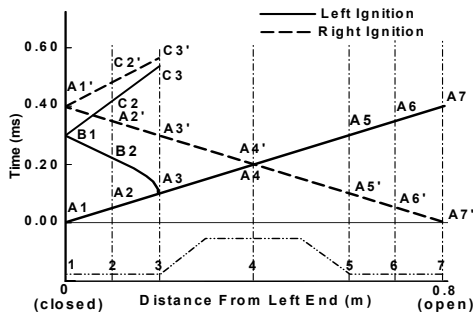


Figure 7: Wave diagram for the two simulated cases: A1-A2-A3-A4-A5-A6-A7 and A1'-A2'-A3'-A4'-A5'-A6'-A7' indicate the detonation wave in the Left Ignition and Right Ignition cases, respectively; A3-B2-B1 and B1-C2-C3 indicate a reflected wave and a secondary reflected wave in segment I in the Left Ignition case; A1'-C2'-C3' indicate a reflection wave in segment I in the Right Ignition case.

The detailed wave profiles show that other waves are induced by area changes. The Left Ignition case is considered first. For is case, Fig. 7 shows a wave denoted as A3-B2-B1 that is reflected off the detonation wave near the exit of the small tube in segment I. This wave moves in the tube, in the opposite direction to that of the detonation wave, and reflects off the closed end wall as B1-C2-C3. This latter wave then moves forward toward the main chamber. Therefore, as shown in Fig. 6, within the given computational time period (0–0.6 ms), the reflection wave A3-B2-B1 causes a pressure increase at Points 1 and 2 (indicated as B1 and B2 respectively) whereas the secondary reflected wave B1-C2-C3 causes a pressure increase at points 2 and 3 (C2 and C3 respectively).

A more detailed examination of the initiation and propagation of the reflected wave and its reflection at the end wall in segment I for the Left Ignition case is provided by Fig. 8, which tracks wave propagation in segment I.

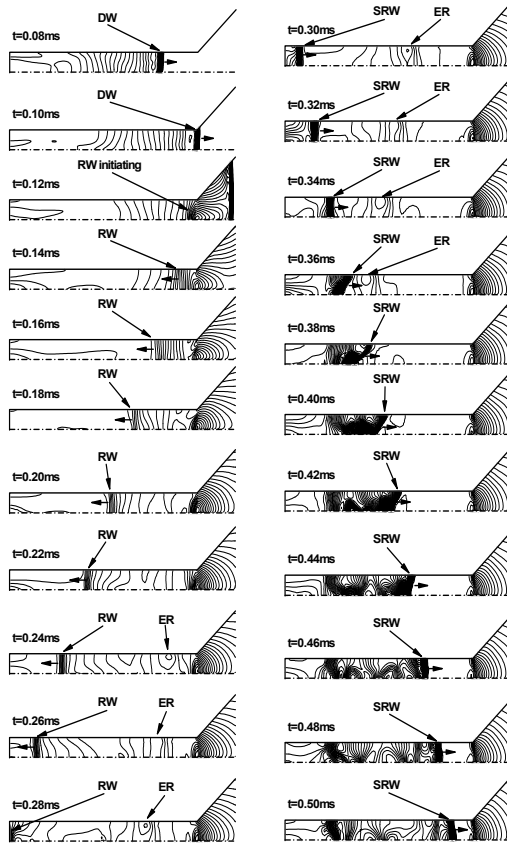


Figure 8: Production and propagation of the reflected wave (DW) and its secondary reflection (SRW) in segment I for Left Ignition case. Pressure contours shown at $t = 0.08-0.50$ ms at 0.02 ms interval: the reflected wave appears at about $t = 0.12$ ms, and reflects by the closed end at about $t = 0.28$ ms. Note an expansion region (ER) exposes in this figure that moves after the reflected wave and then collides with the secondary reflected wave. DW indicates detonation wave.

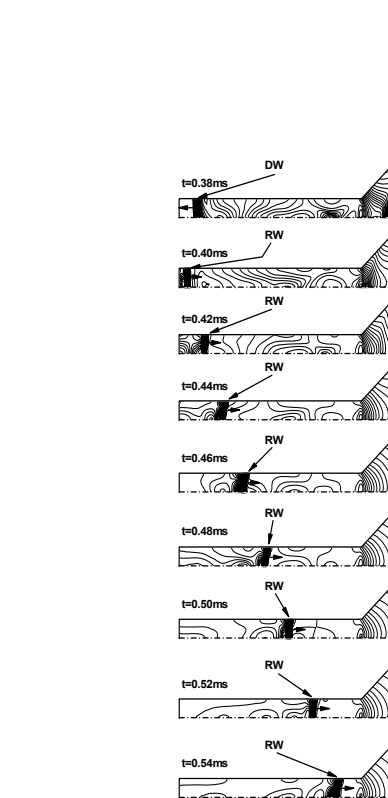


Figure 9: Production and propagation of a reflected wave (RW) in segment I for Right Ignition case. Pressure contours shown at $t = 0.38-0.54$ ms at 0.02 ms interval: the reflected wave is initiated at about $t = 0.39$ ms. DW indicates detonation wave.

From this figure and Fig 7, one can see that the first reflected wave is produced at about $t = 0.12$ ms. This wave propagates back toward the closed end with a low velocity. This wave's propagation speed tends to a constant value of approximately 1450 m/s. Upon reflection from the end wall at about $t = 0.28$ ms, the wave second propagates at approximately 835 m/s.

The Right Ignition case shows a somewhat simpler wave system than the Left Ignition case. For this case, there is only an end-wall wave reflection in segment I produced by the incident detonation wave, denoted as A1'-C2'-C3' in Fig. 7. In Fig. 6, we can see that this reflected wave causes an abrupt pressure increase at points 2 and 3 (C2' and C3' respectively) within the computational time period. As for the Left Ignition case, a more detailed examination of this reflected wave can be made using Fig. 9. From the figure, we note that the reflected wave is produced at about $t = 0.39$ ms and propagates toward the main chamber at approximately 1450 m/s.

As can be expected, a detonation process in a variable cross-section chamber should be more complex than that in a simple constant cross-section tube. There appears to be numerous wave disturbances, more than those discussed above, that results in serious non-uniformities and irregular fluctuations. To discuss each of these waves is impossible and beyond the initial aims of this article. Here we only emphasize phenomena that are most noticeable to highlight the complexity of the wave processes. For example, if we review the results shown in Fig 8, during $t = 0.22$ - 0.38 ms, there is a low-pressure region behind the above-mentioned reflected wave. The evolution of this region is more clearly seen in the larger images in Fig. 10. This low-pressure region initiates at the small tube (segment I) exit at $t = 0.22$ ms and can be qualitatively explained by one-dimensional wave dynamics. This expansion region moves relatively slowly inside the small tube (with a velocity of approximately 835m/s) and collides with the second reflected wave (B1-C2-C3 in Fig. 7) at $t = 0.38$ ms. This collision shrinks and annihilates the expansion region, leaving an acoustic wave. Finally, from our analysis, the main contributors to the extreme parameters in the small tube segments for the two detonation processes are summarized in Table 1.

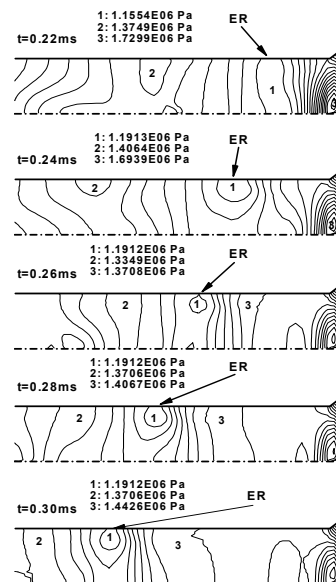


Figure 10: Production of an expansion region (ER) in the small tube area in the Left Ignition case: the same phenomenon can also be seen in Figs.2 and 8.

Table 1: Summary of the main contributors to extreme parameters in the small tube segments

	<i>in Segment I</i>	<i>in Segment II</i>
Left Ignition	Reflected Wave Second Reflected Wave	Tube Convergence
Right Ignition	Tube Convergence Reflected Wave	

C. Propulsion Performance

The complex wave systems propagating in the variable cross-section chamber also has an effect on thrust generation, if such a chamber is configured for propulsion, as in a pulse detonation engine. For a generic detonation tube, the thrust produced by a detonation process can be calculated by the classical formula

$$F(t) = \int_0^S [(p(t) - p_a) + \rho(t)u^2(t)] dS \quad (6)$$

where p_a is the ambient pressure, and $p(t)$, $\rho(t)$ and $u(t)$ are the instantaneous pressure, density and horizontal velocity acting on the thrust wall. In Eq. (6), the integration area S is the area of the walls that the thrust acts on. In our current cases, thrust production occurs on three portions of the tube, as shown in Fig. 11. Besides the portion

yielded on the closed end-wall, F_1 , thrust is also produced on both of the frustums, namely forces F_2 and F_3 . Each thrust portion in our cases can be calculated with the above formula on the associated integration areas.

Impulse is another parameter used to describe the performance of a propulsion system. The impulse is obtained by integrating the thrust from zero to t as

$$I(t) = \int_0^t F(t) dt \quad (7)$$

The specific impulse then can be calculated from the relation

$$I_{sp}(t) = I(t)/(\rho_0 V g) \quad (8)$$

where ρ_0 is the initial density of the reactant gas mixture in the detonation chamber, V is the volume of the chamber, and g is the Earth's sea-level gravitational acceleration. An alternative performance parameter, the fuel-based specific impulse, is also of interest and can be defined as

$$I_{sp,f}(t) = I(t)/(\rho_f V_f g) \quad (9)$$

where ρ_f is the initial density of the gaseous fuel (hydrogen).

The computations for propulsion parameters are performed with a longer period ($t = 0 - 2.5$ ms) to allow the detonation processes to sufficiently exhaust to ambient conditions. The thrusts for each of the detonation cases are shown in Fig. 12. For each case, the first subfigure in Figs. 12(a) and (b) shows the total thrust together with the three thrust portions. The results shown that the detonation processes produce complex thrust histories which may be further understood through observing the behaviors of the three thrust portions. The force F_1 yielded on the closed end-wall, for both detonation cases, is produced by the extreme parameters appearing near the end-wall. The Left Ignition case has relatively constant force F_1 within $t = 0 - 0.28$ ms since the reflected wave A3-B2-B1 stated in Section 4.2 has not yet reached the closed end wall. Thereafter the reflected wave comes and starts to impact the wall, resulting in an abrupt and severe increase in the force level. The higher force level remains for a certain moment and then decays gradually to zero. In the Right Ignition case, a large peak in the force F_1 occurs about 0.4 ms after ignition when the detonation wave reaches the end-wall. The thrust then rapidly decreases to zero.

In both cases, the evolutions of the other two forces F_2 and F_3 are much more complicated. These two forces are first affected by the detonation waves moving through the

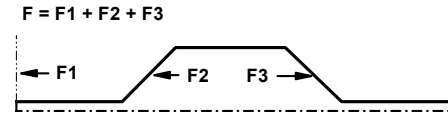


Figure 11: Three portions of the thrust for detonation processes in the chosen variable cross-section chamber.

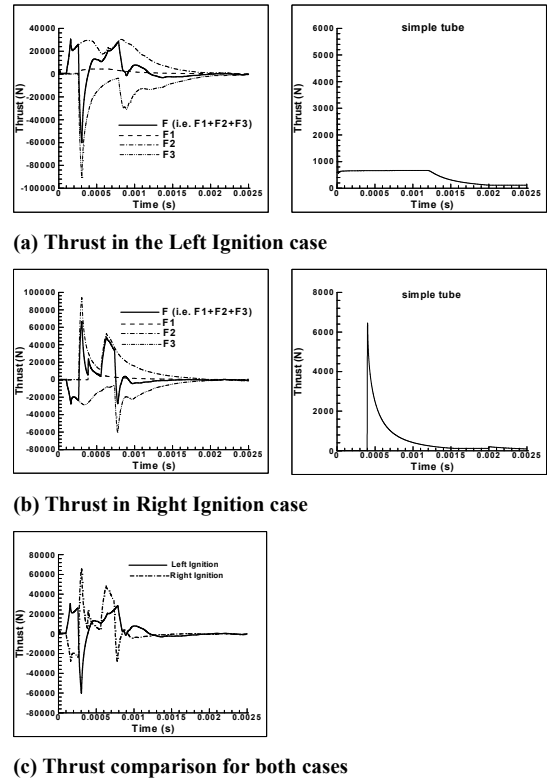


Figure 12: Thrust obtained from simulation of detonation waves in variable cross-section chamber in comparison with a simple (constant cross-section) tube. The simple detonation tube has 20 mm internal radius and 800 mm total length.

corresponding frustums. Consequently, the first abrupt increases or decreases on the forces F_2 and F_3 , respectively, are yielded by detonation waves. Our study shows that reflections off the end-wall have important influences on these two forces. In particular, the Left Ignition case produces the secondary reflected wave B1-C2-C3 that moves through the small tube area (segment I) and may further move forward to the open end. When the wave passes the segment II, it causes the force F_2 to increase at about $t = 0.6$ ms, and the force F_3 to decrease from about $t = 0.8$ ms. The Right Ignition case has the reflected wave A1'-C2'-C3' that also moves through the small tube area (segment I) and may further move forward the open end. When the wave passes segment II, it causes the thrust portion F_2 to increase at about $t = 0.55$ ms, and the thrust portion F_3 to have a decrease at about $t = 0.7$ ms. In both cases, wave propagation through the divergent frustum causes an abrupt decrease in the thrust acting on that frustum (F_2 in Left Ignition case) or increase (F_3 in Right Ignition case) followed by a gradual recovery. Finally, Fig. 12(c) summarizes the thrusts produced by the two cases. The average thrusts for the cases are also calculated by

$$\bar{F} = \int_0^{t_{max}} F(t) dt / t_{max} \quad (10)$$

(where $t_{max} = 2.5$ ms). The results show that the Left Ignition case has an average thrust (3038 N) that is larger than that of the Right Ignition case (2671 N).

The defined impulses for each of the detonation cases are shown in Fig. 13. The Left Ignition and Right Ignition cases show clearly different behaviors initially. Later, the general trends are similar, with the former case performing a little better than the latter.

A comparison was also made between these two cases against detonation wave propagation in a constant section tube, again with the left end closed and for the two cases of left and right ignition. The simple tube has the same internal radius (20 mm) as the small tube in the previous cases. Initial conditions remain the same. The thrust and impulse parameters of the detonation processes for the simple-tube case are also shown in Figs. 12 and 13. The comparison shows the expected result that the variable cross-section chamber yields much higher thrust and thus higher impulse parameters. However, the specific impulses for the variable cross-section chambers are lower due to the larger quantity of reactants for these two cases compared to the straight tube cases.

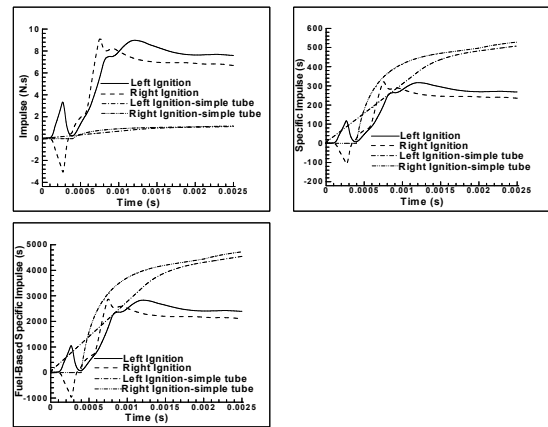


Figure 13: Impulses obtained from simulation of detonation waves in variable cross-section chamber in comparison with a simple tube.

V. Concluding Remarks

A numerical simulation was performed on two-dimensional hydrogen-air detonations occurring in an axis-symmetric variable cross-section combustion chamber. The computational approach used in the simulation is a time-accurate and finite-volume-based method. A five-species and two-step reaction mechanism is adopted to model the thermochemistry of the detonation processes. Two detonation cases, namely, Left and Right Ignition, defined with different initiating locations for the detonations, were studied. The simulation results rebuilt some phenomena that were experimentally observed in Ref. 4. In both simulated detonation processes, extreme parameters within the small tubes were observed. It was thought that reflected waves appearing in the detonations and area reduction were responsible for the extreme parameters. The following facts in the detonation wave were found: in the Left Ignition case, extreme parameters appeared in both small tube segments. In segment V, the extreme parameters were produced by area reduction while in segment I they were produced by multiple wave reflections. In the Right Ignition case, extreme parameters appeared in the small tubes due to a combination of area reduction and wave reflection. Finally, though it is hard to make a comparison of the propulsion performance to decide which case is better than another, the results still showed that the Left Ignition case performed better a little than its partner in the impulse viewpoint.

Acknowledgements

The authors would like to thank Dr. Hyungwon Kim, Agency for Defense Development, Korea, who authored the code, for familiarizing us with the code.

References

- ¹ Kailasanath, K., "Recent developments in the research on pulse detonation engines," *AIAA Journal*, Vol. 41, No. 2, 2003, pp. 145–159.
- ² Lu, F. K., Wilson, D. R., Bakos, R. and Erdos, J. I., "Recent advances in detonation techniques for high-enthalpy facilities," *AIAA Journal*, Vol. 38, No. 9, 2000, pp. 1676–1684.
- ³ Kim, H., Lu, F. K., Anderson, D. A. and Wilson, D. R., "Numerical simulation of detonation process in a tube," *Computational Fluid Dynamics Journal*, Vol. 12, No. 2, 2003, pp. 227–241.
- ⁴ Baklanov, D. I., Gvozdeva, L. G. and Scherbak, N. B., "Formation of high-speed gas flow at combustion in the regime of multi-step detonation," in G. Roy, S. Frolov, K. Kailasanath and N. Smirnov (eds.), *Gaseous and Heterogeneous Detonations, Science to Application*, ENAS Publishers, Moscow, 1999, pp. 141–152.
- ⁵ Baklanov, D.I. and Gvozdeva, L.G., "Nonstationary processes during propagation of detonation waves in channels of variable cross section," *High Temperature*, Vol. 33, No. 6, 1995, pp. 955–958.
- ⁶ Baklanov, D.I. and Gvozdeva, L.G., "The effect of additional ignition on the stability of emergence of the mode of double nonstationary discontinuity in combustors," *High Temperature*, Vol. 34, No. 2, 1996, pp. 294–297.
- ⁷ Gnoffo, P. A., Gupta, R. N. and Shinn, J. L., "Conservation equations and physical models for hypersonic air flows in thermal and chemical nonequilibrium," NASA TP-2867, 1989.
- ⁸ Candler, G. V., "The Computation of Weakly Ionized Hypersonic Flows in Thermo-Chemical Nonequilibrium," Ph.D. Dissertation, Stanford University, June 1988.
- ⁹ Vincenti, W. G. and Kruger, C. H., Jr., *Introduction to Physical Gas Dynamics*, Krieger, Malabar, Florida, 1977.
- ¹⁰ Millikan, R. C. and White, D. R., "Systematics of Vibrational Relaxation," *Journal of Chemical Physics*, Vol. 39, No. 12, 1963, pp. 3209–3213.
- ¹¹ Roe, P. L., "Approximate Riemann solvers, parameter vectors, and difference schemes," *Journal of Computational Physics*, Vol. 43, No. 2, 1981, pp. 357–372.
- ¹² Grossman, B. and Cinnella, P., "Flux-split algorithms for flows with nonequilibrium chemistry and vibrational relaxation," *Journal of Computational Physics*, Vol. 88, No. 1, 1990, pp. 131–168.
- ¹³ Rogers, R. C. and Chinitz, W., "Using a global hydrogen-air combustion model in turbulent reacting flow calculations," *AIAA Journal*, Vol. 21, No. 4, 1983, pp. 586–592.
- ¹⁴ Rudinger, G., *Wave Diagrams for Nonsteady Flow in Ducts*, Van Nostrand, New York, 1955.